A novel first principles approach for the estimation of the sieve factor of blood samples

L. Northam* and G. V. G. Baranoski
Natural Phenomena Simulation Group, School of Computer Science, University of Waterloo
200 University Avenue West, Waterloo, Ontario, N2L 3G1, Canada
**lanortha@uwaterloo.ca*

Abstract: Light may traverse a turbid material, such as blood, without encountering any of its pigment containing structures, a phenomenon known as sieve effect. This phenomenon may result in a decrease in the amount of light absorbed by the material. Accordingly, the corresponding sieve factor needs to be accounted for in optical investigations aimed at the derivation of blood biophysical properties from light transmittance measurements. The existing procedures used for its estimation either lack the flexibility required for practical applications or are based on general formulas that incorporate other light and matter interaction phenomena such as detour (scattering) effects. In this paper, a ray optics framework is proposed to estimate the sieve factor for blood samples. It employs a first principles approach to account for the distribution, orientation and shape of the cells that contain hemoglobin, the essential (oxygen-carrying) pigment found in human blood. Within this framework, ray-casting techniques are used to determine the probability that light can traverse a blood sample without encountering any of these cells. The predictive capabilities of the proposed framework are demonstrated through a series of *in silico* experiments. Its effectiveness is further illustrated by visualizations depicting the different blood parameterizations considered in the simulations.

OCIS codes: (170.7050) Turbid media; (000.5490) Probability theory, stochastic processes, and statistics.

References and links

1. A. Amelink, T. Christiaanse, and H. J. C. M. Sterenborg, "Effect of hemoglobin extinction spectra on optical spectroscopic measurements of blood oxygen saturation," Opt. Lett. **34**, 1525–1527 (2009).
2. P. Agache, "Assessment of erythema and pallor," in "Measuring the Skin," , P. Agache and P. Humbert, eds. (Springer-Verlag, Berlin, 2004), pp. 591–601.
3. A. N. Yaroslavsky, A. V. Priezzhev, J. Rodriquez, I. V. Yaroslavsky, and H. Battarbee, *Optics of Blood* (SPIE-Press, Bellingham, 2002).
4. V. V. Tuchin, *Tissue Optics Light Scattering Methods and Instruments for Medical Diagnosis* (The International Society for Optical Engineering, Bellingham, 2000).
5. W. M. Star, "Light dosimetry in vivo," Phys. Med. Biol. **42**, 763–787 (1997).
6. Y. M. Serebrennikova, J. M. Smith, D. E. Huffman, G. F. Leparc, and L. H. García-Rubio, "Quantitative interpretations of visible-nir reflectance spectra of blood," Opt. Express **16**, 18215–18229 (2008).
7. V. V. Barun and A. P. Ivanov, "Effect of hemoglobin localization in erythrocytes on optical absorption by human blood," in "Tenth International Conference on Light Scattering by Non-spherical Particles," (Bodrun, Turkey, 2007), pp. 5–8.

#123519 - $15.00 USD Received 29 Jan 2010; revised 11 Mar 2010; accepted 15 Mar 2010; published 25 Mar 2010

8. J. Laufer, D. T. Delpy, C. Elwell, and P. Beard, "Quantitative spatially resolved measurment of tissue chromophore concentrations using photoacoustic spectroscopy: application to the measurement of blood oxygenation and haemoglobin concentration," Phys. Med. Biol. **52**, 141–168 (2007).
9. D. Eng and G. Baranoski, "The application of photoacoustic absorption spectral data to the modeling of leaf optical properties in the visible range," IEEE Trans. Geosci. Remote Sens. **45**, 4077–4086 (2007).
10. W. L. Butler, "Absorption spectroscopy in vivo: Theory and applications," Ann. Rev. Plant Physiol. **15**, 451–470 (1964).
11. T. C. Vogelmann, "Plant Tissue Optics," Annu. Rev. Plant Physiol. Mol. Biol. **44**, 231–251 (1993).
12. D. T. Delpy, M. Cope, P. van der Zee, S. Arridge, S. Wray, and J. Wyatt, "Estimation of optical pathlength through tissue from direct time of flight measurement," Phys. Med. Biol. **33**, 1433–1442 (1988).
13. S. J. Matcher, M. Cope, and D. T. Delpy, "Use of the water absorption spectrum to quantify tissue chromophore concentration changes in near-infrared spectroscopy," Phys. Med. Biol. **39**, 177–196 (1994).
14. E. I. Rabinowitch, *Light absorption by pigments in the living cell* (Interscience Publishers Inc., New York, 1951), vol. II, chap. 22.
15. W. Rühle and A. Wild, "The intensification of absorbance changes in leaves by light dispersion," Planta **146**, 551–557 (1979).
16. L. Fukshansky, *Optical properties of plants* (Academic Press, London, 1981).
17. G. Baranoski and D. Eng, "An investigation on sieve and detour effects affecting the interaction of collimated and diffuse infrared radiation (750 to 2500 nm) with plant leaves," IEEE Trans. Geosci. Remote Sens. **45**, 2593–2599 (2007).
18. J. Evans, T. Vogelmann, and W. Williams, "Chloroplast to leaf," in "Photosynthetic Adaptation Chloroplast to Landscape," , W. Smith, T. Vogelmann, and C. Critchley, eds. (Springer, NY, USA, 2004), chap. 2, pp. 15–41. Part 2: Sunlight Capture, Ecological Studies, Vol. 178.
19. F. Garlaschi, G. Zucchelli, and R. Jennings, "Studies on light absorption and photochemical activity changes in chloroplast suspensions and leaves due to light scattering and light filtartion across chloroplasts and vegetation layers," Photosynthesis Research **20**, 207–220 (1989).
20. L. N. M. Duysens, "The flattening of the absorption spectrum of suspensions as compared to that of solutions," Biochim. Biophys. Acta **19** (1956).
21. R. N. Pittman, "In vivo photometric analysis of hemoglobin," Ann. Biomed. Eng. **14**, 1416–1432 (1986).
22. L. Fukshansky, "On the theory of light absorption in non-homogeneous objects," J. Math. Biol. **6**, 1416–1432 (1978).
23. J. M. Steinke and A. P. Shepherd, "Comparison of mie theory and the light scattering of red blood cells," Appl. Opt. **27**, 4027–4033 (1988).
24. A. T. Lovell, J. C. Hebden, J. C. Goldstone, and M. Cope, "Determination of the transport scattering coefficient of red blood cells [3597-121]," in "Society of Photo-Optical Instrumentation Engineers (SPIE) Conference Series," , vol. 3597, B. Chance, R. R. Alfano, and B. J. Tromberg, eds. (1999), vol. 3597, p. 175.
25. M. Meinke, G. Müller, J. Helfmann, and M. Friebel, "Optical properties of platelets and blood plasma and their influence on the optical behavior of whole blood in the visible to near infrared wavelength range," J. Biomed. Opt. **12**, 014024 (2007).
26. K. Kramer, J. Elam, G. Saxton, and W. E. Jr., "Influence of oxygen saturation, concentration and optical depth upon the red and near-infrared light transmittance of whole blood," Am. J. Physiology **165**, 229–246 (1951).
27. L. Northam, "A ray optics framework for the computation of the sieve effect factor for blood," Master's thesis, University of Waterloo, Waterloo, Ontario (2010).
28. T. Wriedt, J. Hellmers, E. Eremina, and R. Schuh. "Light scattering by single erythrocyte: Comparison of different methods", J. Quant. Spectrosc. Radiat. Transfer **100**, 444456 (2006).
29. R. Skalak and P. I. Branemark, "Deformation of Red Blood Cells in Capillaries," Science **164**, 717–719 (1969).
30. S. Chei, M. Boyer, J. Meng, D. Tarjan, J. W. Sheaffer, and K. Skadron, "A performance study of general-purpose applications on graphics processors using cuda," J. Parallel Distrib. Comput. **68**, 1370–1380 (2008).
31. L. Orf, "Scientific visualizations with pov-ray," Linux J. **2004**, 2 (2004).
32. N. M. Anderson and P. Sekelj, "Light-absorbing and scattering properties of nonhaemolysed blood," Phys. Med. Biol. **12**, 173–184 (1967).
33. N. M. Anderson and P. Sekelj, "Reflection and transmission of light by thin films of nonhaemolysed blood," Phys. Med. Biol. **12**, 185–192 (1967).
34. M. Meinke, G. Müller, J. Helfmann, and M. Friebel, "Empirical model functions to calculate hematocrit-dependent optical properties of human blood," Appl. Opt. **46**, 1742–1753 (2007).
35. A. N. Yaroslavsky, I. V. Yaroslavsky, T. Goldbach, and H. J. Schwarzmaier, "Influence of the scattering phase function approximation on the optical properties of blood determined from the integrating sphere measurements," J. Biomed. Opt. **4**, 47–53 (1999).
36. S. T. Flock, B. C. Wilson, and M. S. Patterson, "Total attenuation coefficient and scattering phase function of tissues and phantom materials at 633nm," Med. Phys. **14**, 1742–1753 (1987).
37. M. Hammer, D. Schweitzer, B. Michel, E. Thamm, and A. Kolb, "Single scattering by red blood cells," Appl. Opt. **37**, 7410–7418 (1998).

#123519 - $15.00 USD Received 29 Jan 2010; revised 11 Mar 2010; accepted 15 Mar 2010; published 25 Mar 2010

38. A. Roggan, M. Friebel, K. Doershel, A. Hahn, and G. Mueller, "Optical properties of circulating human blood in the wavelength range 400-2500nm," J. Biomed. Opt. **4**, 36–46 (1999).
39. E. G. Popov, "Orientation of nonspherical cells in blood flowing through a vessel," Bull. Exp. Biol. Med. **86**, 1556–1557 (1978).
40. J. H. McClendon and L. Fukshansky, "On the interpretation of absorption spectra of leaves - ii. the non-absorbed ray of the sieve effect and the mean optical pathlength in the remainder of the leaf," Photochem. Photobiol. **51**, 211–216 (1990).
41. B. D. Ventura, C. Lemerle, K. Michalodimitrakis, and L. Serrano, "From *in vivo* to *in silico* biology and back," Nature **443**, 527–533 (2006).

1. Introduction

The study of the optical properties of blood is essential for a wide scope of biomedical applications. Examples range from the assessment of hemoglobin concentration and oxygenation levels [1] to the measurement and interpretation of photobiophysical responses of human tissues [2]. Accordingly, the investigation of light interactions with blood has always been one of the focal points of biomedical optics research [3]. In the last decades, computer simulations or *in silico* experiments, paired with traditional "wet" experiments, are increasingly being employed in these investigations. The information derived from these simulations, in turn, is being used to support the noninvasive measurement of tissue optical properties required for the diagnosis [4] and treatment of diseases [5].

One of the main components of these *in silico* investigations refers to the modeling of light absorption by organic pigments or absorbers, such as hemoglobin, in order to derive biophysical properties through inversion procedures [6–8]. The pigments' absorption spectra used in this task are usually obtained under *in vitro* conditions, *i.e.*, their extinction coefficients are computed using light transmission measurements performed in homogeneous solutions in which these pigments (or chromophores) are uniformly distributed [9]. However, in their native (*in situ*) state, natural pigments (*e.g.*, hemoglobin and chlorophyll) are found in cells or organelles. As a result, when light traverses the material, refractive index differences between cell walls and intercellular medium may cause multiple internal reflections that increase the light optical pathlength, which, in turn, increases the probability of light absorption. This lengthening of the optical pathlength is referred to as the detour effect [10, 11]. To account for changes in the lengthening of the optical pathlength under *in situ* conditions when using *in vitro* absorption (or extinction) curves, several researchers choose to employ a parameter, known as the differential pathlength factor [12, 13], to scale these curves.

The distribution of absorbers within a target material can also have an opposite effect on the light absorption. More specifically, light traversing the material may not encounter any of its pigment containing structures (Fig. 1), a phenomenon known as sieve effect [11, 14]. This phenomenon, also called "pure" sieve effect since it does not involve light interactions (scattering) with pigment containing structures [16], reduces the probability of light absorption. It has been well documented [15–18] that detour and sieve effects not only have opposite influences in the absorption profile of turbid materials, but they are also more pronounced in different regions of the light spectrum. While a higher or increased rise in absorption values caused by the detour effect is more noticeable in bands of absorption minima [19], the lower or decreased rise in absorption values caused by the sieve effect is more noticeable in bands of absorption maxima [14]. For this reason, the sieve effect is also known as the absorption flattening effect [20] since the peaks in the absorption spectra of the pigments in their native state are depressed relative to the peaks for a homogeneous solution with the same average pigment concentration [21]. Despite its importance, the estimation of sieve effect has received considerably less attention than the estimation of detour effect in the scientific literature.

The formulas that have been proposed to estimate a factor that quantifies this effect [15, 20–

#123519 - $15.00 USD Received 29 Jan 2010; revised 11 Mar 2010; accepted 15 Mar 2010; published 25 Mar 2010

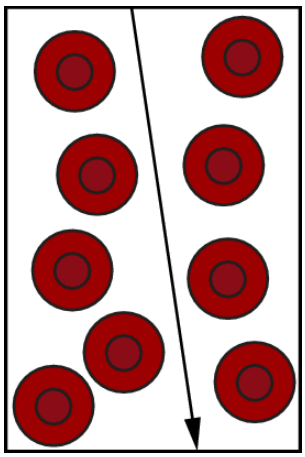

Fig. 1. Light traversing a medium may not encounter any of the pigment containing structures present in this medium, a phenomenon known as sieve effect.

22] usually lack the flexibility to efficiently account for changes in the shape and orientation of the pigment containing structures, and rely on measured values that may be unavailable. McClendon and Fukshansky (1990) suggested that a direct and more accurate estimation of the sieve factor for an organic tissue could be possible through a detailed examination of its anatomy. To the best of our knowledge, however, such a direct approach has not been yet presented in the biomedical literature.

In this paper, we propose a novel ray optics framework for the computation of the sieve factor for blood samples. It overcomes the practical constraints of previous methods by using a first principles approach. This approach consists in geometrically modeling the main pigment containing structures, namely the red blood cells (RBCs) or erythrocytes, and applying ray-casting techniques to compute the probability of a light ray intersecting these cells as it traverses a blood sample. The RBCs are modeled using a new and cost-effective three-dimensional representation that closely approximates their biconcave disk shape. We remark that these cells are the primary absorbers and scatterers within whole blood [23], and they are largely responsible for its optical behavior [24, 25]. We computed the sieve factor for several blood samples with varying thickness and hematocrit (percentage of blood volume occupied by red blood cells) using the proposed framework to demonstrate its predictability and effectiveness. In addition, we employed different cell shapes and orientations in our *in silico* experiments to illustrate the dependence of sieve effect factors on the geometry and distribution of the erythrocytes.

2. Methods

2.1. Background

The transmittance of light traversing a homogeneous solution at a wavelength λ can be obtained using the Beer-Lambert law [16]:

$$T(\lambda) = \frac{\Phi_t(\lambda)}{\Phi_i(\lambda)} = e^{-\varepsilon(\lambda)cd}, \tag{1}$$

where Φ_t/Φ_i corresponds to the ratio of incident to transmitted flux, ε and c are the extinction coefficient and the concentration of the absorbing substance (pigment) respectively, and d is the optical pathlength through the sample.

#123519 - $15.00 USD Received 29 Jan 2010; revised 11 Mar 2010; accepted 15 Mar 2010; published 25 Mar 2010

Inverting Eq. (1) yields Eq. (2), the optical density:

$$D(\lambda) = \ln\left(\frac{\Phi_i(\lambda)}{\Phi_t(\lambda)}\right) = \varepsilon(\lambda)cd. \tag{2}$$

In order to compute the optical density of a turbid material such as blood, one can employ a modified version of the Beer-Lambert law given by Eq. (3):

$$D(\lambda) = \ln\left(\frac{\Phi_i(\lambda)}{\Phi_t(\lambda)}\right) = \beta(\lambda)\varepsilon(\lambda)cd, \tag{3}$$

where β corresponds to a scale factor to account for sieve and detour effects.

The scale factor denoted by β is called differential pathlength factor in studies involving human tissues [12] and ratio or factor of intensification in studies involving plant tissues [15]. While in the former it is usually associated only with the lengthening of the optical pathlength due to detour effects, in the latter it also includes the influence of possible sieve effects that could decrease light absorption [15]. For completeness, we adopt the latter description in this paper, *i.e.*, we define β as $\beta_s\beta_d$, where β_d corresponds to the detour factor and β_s corresponds to the sieve factor, the focus of this investigation. It is important to note that the sieve effect is wavelength independent [14] since it corresponds to the absense of light interactions with absorbers.

In the literature, several formulas exist for the computation of the sieve factor. For example, Duysens (1956) and Pittman (1986) proposed the following expression:

$$\beta_s = \frac{D_{sus}(\lambda)}{D_{sol}(\lambda)}, \tag{4}$$

where D_{sus} and D_{sol} correspond to the optical densities of the pigment in suspension and in solution respectively. If a measured value for D_{sus} is unknown, it is replaced by an approximated value. For example, Duysens (1956) provided approximations for suspensions composed of cubical, spherical and arbitrary shaped particles, and Pittman (1986) provided the following formulas [Eqs. (5) and (6)] to approximate the optical density of red blood cells in suspension:

$$D_{sus}(\lambda) = m\log_{10}\left[1 - aH(1 - 10^{-\varepsilon(\lambda)c_h b})\right], \tag{5}$$

and the optical density of hemoglobin in solution:

$$D_{sol}(\lambda) = \varepsilon(\lambda)c_h Hd, \tag{6}$$

where c_h is the concentration of hemoglobin in a red blood cell, H is the hematocrit, a is the cellular shape factor, m is the number of cell layers, and b is the average pathlength through a red blood cell.

Another formula [Eq. (7)] to estimate the sieve effect factor was provided by Fukshansky (1978):

$$\beta_s = \frac{D_{sol}(\lambda) - D_{sus}(\lambda)}{D_{sol}(\lambda)}, \tag{7}$$

where

$$D_{sus}(\lambda) = -\ln\left((1-\gamma) + \gamma e^{-\frac{1}{\gamma}D(\lambda)_{sol}}\right), \tag{8}$$

and γ corresponds to the fractional area occupied by the pigment containing structures.

We remark that these sieve factor estimation formulas rely on the availability of measured data. Furthermore, the approximations for optical density given in Eqs. (5) and (8) do

#123519 - $15.00 USD Received 29 Jan 2010; revised 11 Mar 2010; accepted 15 Mar 2010; published 25 Mar 2010

not account for changes in shape, distribution or orientation of the pigment containing structures. Finally, recall that the sieve factor corresponds to the probability that light does not encounter the absorbers, *i.e.*, $0 \leq \beta_s \leq 1$. However, if $D_{sus}(\lambda) \geq D_{sol}(\lambda)$ (which may be true for blood [24,26]), then $\beta_s = D_{sus}(\lambda)/D_{sol}(\lambda) \geq 1$. This indicates that the estimation provided by Eq. (4) also includes detour effects. In fact, Duysens (1956) and Pittman (1986) state that the ratio $D_{sus}(\lambda)/D_{sol}(\lambda)$ depends on the amount of light absorbed by the cells, which is only possible if one accounts for the light interactions (scattering) with the pigment containing structures (RBCs). Since by definition [11,14,16] sieve effect does not involve such interactions, it is clear that this ratio incorporates detour (scattering) effects, which by definition [10,11] account for such interactions. Similar observations with respect to other natural pigments (*e.g.*, chlorophyll) have been reported in the literature [15]. In the proposed framework, which is described in the following section, the limitations outlined above are addressed through the application of a first principles approach.

2.2. Framework

The proposed framework combines ray optics concepts with ray casting techniques to obtain an estimate for the sieve factor of blood samples contained in a testing volume. In this section, we describe the general algorithm and blood-specific parameterizations used in our simulations, and outline relevant implementation issues.

2.2.1. General Algorithm

A Monte Carlo based algorithm is employed in our *in silico* experiments, and its basic steps are summarized as follows:

1. initialize no-hits counter $n = 0$
2. generate and randomly distribute cells within the test volume according to user-specified parameters defining the experimental conditions
3. compute the number of cells intersecting a ray sent through the volume
4. if no cells are intersected by the ray, increment n
5. repeat steps 2-4 N times
6. compute sieve factor $\beta_s = n/N$

The main reason for randomly varying the distribution of the cells within the whole sample volume at each iteration is to closely approximate the actual three-dimensional arrangement of the RBCs along the ray path. In a given experiment, these cells occupy a certain percentage (given as an hematocrit value) of the sample volume. If we choose to consider only a small section of this volume along the ray path, then we have to deal with a smaller number of cells. The distribution of the cells in this region, however, is affected by the distribution of the cells within the whole volume. For example, for a given blood sample characterized by a hematocrit of 5%, we know that 5% of the volume is occupied by the RBCs. However, there are regions of this volume occupied by many cells, and others that are occupied by few cells. As a result, a ray traversing a very populated region will have a high probability to hit a cell, while a the ray traversing a scarcely populated region will have a low probability to hit a cell. Since we do not know *a priori* the number and the geometrical arrangement of the cells along the ray path, we need to consider their distribution with respect to whole sample volume. Furthermore, by also varying the ray entrance point in the sample volume at each iteration, we can obtain asymptotically convergent results in a faster rate [27]. In order to choose different entrance

#123519 - $15.00 USD Received 29 Jan 2010; revised 11 Mar 2010; accepted 15 Mar 2010; published 25 Mar 2010

points for a ray without introducing any bias in the Monte Carlo simulations, it is necessary to consider the distribution of the cells within the whole sample volume.

2.2.2. Testing Volume

Volume size affects algorithm performance since cell count is proportional to volume. For example, a $1.0mm^3$ sample of human blood with hematocrit equal to 5% contains approximately 5×10^5 red blood cells [3]. It would be computationally expensive to consider such a volume since 5×10^5 ray-cell intersection tests would be required per iteration. Hence, to reduce cell count, we selected a rectangular prism volume with dimensions given by $0.1mm \times 0.1mm \times t$, where t corresponds to the blood sample thickness.

2.2.3. Cell Geometry

Although red blood cells resemble biconcave disks [3], they are usually approximated by simple objects, such as volume or surface area equivalent spheres [3, 23], in studies involving the optical properties of whole blood. In simulations of light scattering by a single RBC, more elaborated objects are used to represent its biconcave disk shape. For a review of these objects, the interested reader is referred to the work by Wriedt et al. (2006). Although these objects could be employed in the proposed framework, they would substantially decrease performance since the computation of ray intersections with these objects would require the solution of complex equations. Alternatively, these objects could be tessellated into simpler primitives (*e.g.*, triangles). In this case, one would have to solve simple equations. However, in order to keep the representations accurate, one would also have to tessellate each object into a large number of primitives (on the order of thousands [28]). This would make the computation of ray-cell intersections $O(cp)$ instead of $O(c)$, where c and p correspond to the number of cells and the number of primitives respectively. In other words, thousands of intersections tests (one per each primitive) would need to be computed per cell to determine the actual ray-cell intersection point.

In our *in silico* experiments, we employed an representation for the RBCs that consists in the union of a torus with a cylinder, herein referred to as the TUC-cell (Fig. 2). It closely approximates the overall biconcave disk shape of RBCs, and allows the computation of ray-cell intersections (three per cell) through the solution of simple and cost-effective equations associated with the standard geometrical primitives that form the TUC-cell. It is important to note that not all erythrocytes have exactly the same shape, and small deviations from the standard biconcave disk shape are expected specially due to micro and macro environmental changes. For example, during certain flow conditions [29], these cells change into a parachute like shape without large variations in their overall length or forward end during acceleration from rest. However, data quantitatively describing these shape deviations is not readily available in the literature. Hence, for the purpose of this investigation, it is assumed that all cells have the same shape, and the propagation of light through the samples is performed under steady-state environmental conditions.

The volume of a TUC-cell was computed taking into account the geometry described in Fig. 2, and considering the volume of the torus added to a volume of revolution defined by the volume of the cylinder not inside the torus. The resulting expression is given by:

$$V_{TUC} = 2\pi^2 R r^2 + 2\pi \left[rR^2 \sin x - r^2 R \left(\frac{1}{2}x + \frac{1}{4}\sin(2x) \right) + r^3 \left(\frac{1}{3}(2+\cos^2 x)\sin x \right) \right], \quad (9)$$

where

$$x = \sin^{-1}\left(\frac{h/2}{r}\right). \quad (10)$$

#123519 - $15.00 USD Received 29 Jan 2010; revised 11 Mar 2010; accepted 15 Mar 2010; published 25 Mar 2010

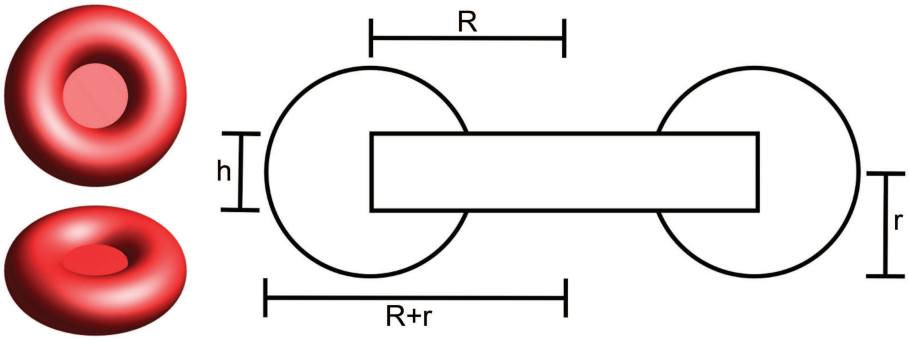

Fig. 2. Dimensions of a TUC-cell. On the left, raytraced views of the final shape. On the right, a cross-section of the TUC-cell showing the dimensions of the torus and cylinder. Cylinder has radius $R = 2.62\mu m$, and height $h = 0.81\mu m$. Torus has major radius $R = 2.62\mu m$, and minor radius $r = 1.29\mu m$ (diameter $2r = 2.58\mu m$). The radius of the TUC-cell is given by $R + r = 3.91\mu m$.

The dimensions of a TUC-cell, given by $r = 1.29\mu m$, $R = 2.62\mu m$ and $h = 0.81\mu m$, were selected according to physiological limits provided in the literature [3]. As a result, the volume computed for the TUC-cell ($90.7\mu m^3$) using Eq. (9) is within the physiological range provided for the volume of an actual red blood cell, namely $94 \pm 14\mu m^3$ [3, 23].

2.2.4. Generation and Distribution of TUC-Cells

Given the testing volume (V_{prism}) and hematocrit (H), the number of TUC-cells (K) to be generated is computed using Eq. (11) :

$$K = H\frac{V_{prism}}{V_{TUC}}. \tag{11}$$

The generated TUC-cells are randomly distributed throughout the volume obeying the following rules:

1. a TUC-cell must exist entirely within the volume, and
2. TUC-cells cannot overlap.

Collision detection is performed for each TUC-cell prior to placement, preventing overlaps. This operation is simplified by encompassing each cell in a bounding volume, and then testing for intersections between bounding volumes. After the TUC-cells are distributed, their bounding volumes are removed and play no part in the actual computation of the sieve factor.

The procedure employed for collision detection has two main phases. Phase 1 tests for collision between bounding spheres (with radius $R + r$). If a collision between bounding spheres is detected, then phase 2 is executed. In phase 2, collision detection is performed using a bounding shape for the TUC-cell, henceforth referred to as "sphere pack" (Fig. 3). This shape was selected due its higher accuracy/cost ratio (compared to cylinders or torii) with respect to collision computations. The sphere pack consists of three circular planes or "plates" (top, middle and bottom with radii equal to R, $R + r$ and R respectively), and a ring of spheres (with radius r).

2.2.5. Implementation Issues

The stochastic nature of the proposed simulation algorithm requires a large numbers of iterations, *i.e.*, N has to be large enough to guarantee asymptotically convergent results. In our

#123519 - $15.00 USD Received 29 Jan 2010; revised 11 Mar 2010; accepted 15 Mar 2010; published 25 Mar 2010

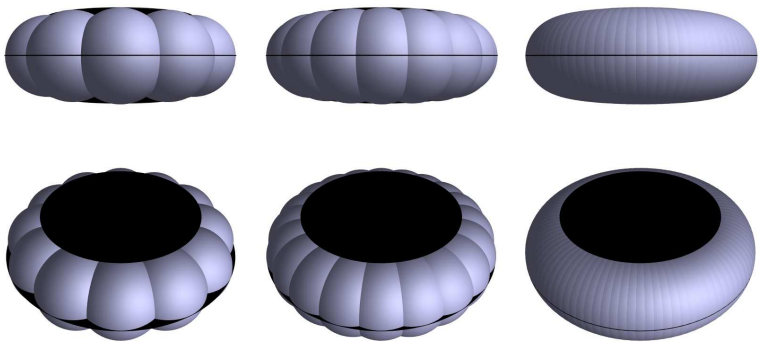

Fig. 3. Images describing the ”sphere pack” bounding shape used to detect collisions between TUC-cells. On the left, 12 spheres are used; in the middle, 20 spheres; and on the right, 100 spheres. Top and bottom images represent the same object viewed from different angles. Note that by increasing the number of spheres forming the ring, the smoother the bounding shape becomes. However, increasing sphere count decreases the performance of the collision detection procedure.

experiments, we used $N = 10^5$. Hence, the estimation of the sieve factor may become computationally expensive. However, the algorithm iterations are independent (Section 2.2.1), and therefore parallelizable. Accordingly, we implemented the proposed algorithm on the CUDA platform [30], a massively multi-threaded computational environment in which thousands of ray-cell intersection tests can be done in parallel.

We also generated images to further illustrate our *in silico* experiments and to broaden the analysis of their results. These images were rendered using the open-source ray-tracing simulation package “POV-Ray 3.6” [31].

2.3. Experimental Set-Up

Three sets of experiments were conducted. In each set, a different sample thickness ($0.1mm$, $0.25mm$ and $1.0mm$) was adopted, and three representations for the erythrocytes, namely volume equivalent spheres, randomly oriented TUC-cells (simulating agitated blood) and flow oriented TUC-cells, were used to compute the sieve factor for samples with hematocrits varying between 1% and 10%. The values selected for these experimental parameters are consistent with blood optical investigations described in the literature (Table 1).

Table 1. Summary of biophysical parameters employed to describe the different *in silico* experimental conditions considered in this investigation.

Parameter	Default Value	Range	Source
Sample Thickness	$0.1mm$	$0.1mm$–$1.0mm$	[23, 32–37]
Hematocrit	5%	1–10%	[23, 34, 36–38]
Orientation	random	random, flow	[29, 39]

The light incidence direction is assumed to be perpendicular to the top face of testing volume, *i.e.*, it is parallel to the main axis of the flow oriented TUC-cells. It is important to note that a flow oriented TUC-cell is characterized by having the plane containing its main axis perpendicular to the flow direction [29, 39]. We remark that this orientation only affects TUC-cells since volume equivalent spheres are symmetrical.

#123519 - $15.00 USD Received 29 Jan 2010; revised 11 Mar 2010; accepted 15 Mar 2010; published 25 Mar 2010

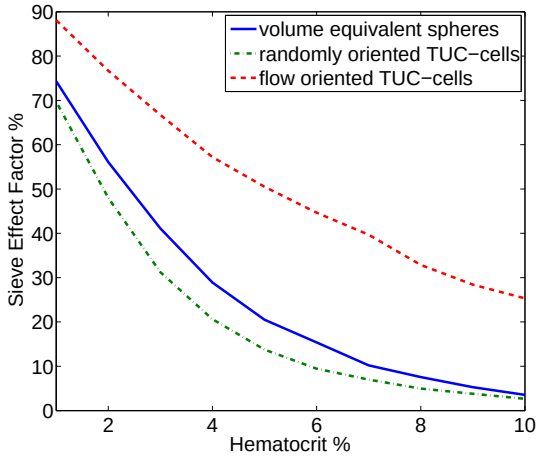

Fig. 4. Plots of sieve effect factors computed for blood samples with thickness equal to $0.1mm$. Three representation for the erythrocites were considered in these experiments: volume equivalent spheres, randomly oriented TUC-cells and flow oriented TUC-cells.

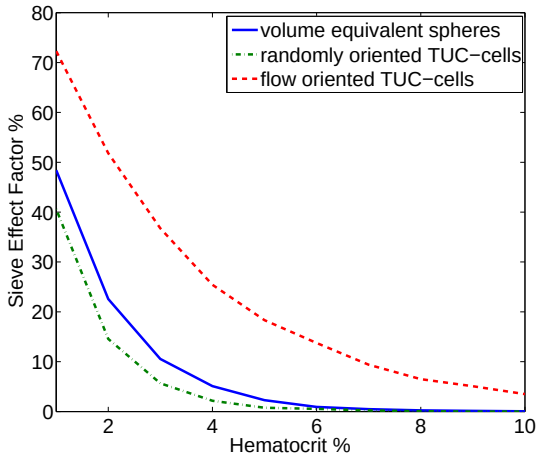

Fig. 5. Plots of sieve effect factors computed for blood samples with thickness equal to $0.5mm$. Three representation for the erythrocites were considered in these experiments: volume equivalent spheres, randomly oriented TUC-cells and flow oriented TUC-cells.

3. Results and Discussion

An increase in the number of erythrocytes decreases the amount of unoccupied space within the volume of blood sample, which, in turn, increases the probability of light intersecting these cells. Hence, the sieve factor is expected to decrease as hematocrit increases [21]. As can be observed in the plots presented in Figs. 4, 5, and 6, the results provided by the proposed framework are consistent with this trend.

Similarly, the sieve factor is expected to be higher for volume equivalent spheres because their surface area and profile are smaller than those of a TUC-cell. Visually, a cell profile cor-

#123519 - $15.00 USD Received 29 Jan 2010; revised 11 Mar 2010; accepted 15 Mar 2010; published 25 Mar 2010

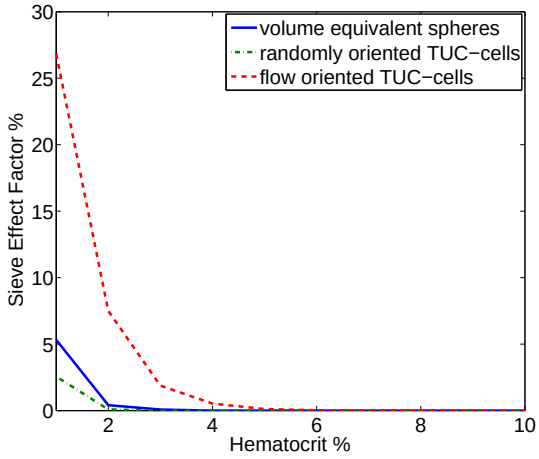

Fig. 6. Plots of sieve effect factors computed for blood samples with thickness equal to 1.0*mm*. Three representation for the erythrocites were considered in these experiments: volume equivalent spheres, randomly oriented TUC-cells and flow oriented TUC-cells.

responds to the area occupied by a cell when projected onto a plane, *i.e.*, a TUC-cell lying flat on a table appears to occupy more space than a volume equivalent sphere when looking down onto the table. As can be observed in the plots depicted in Figs. 4, 5, and 6, the results provided by the proposed framework are also consistent with this trend.

It has long been determined that the sieve effect is smaller when the pigment containing structures have an uniform (parallel) random distribution with respect to the light incidence direction [14]. Accordingly, the sieve factor is expected to be higher for flow oriented TUC-cells in comparison with randomly oriented (agitated) TUC-cells. As it can be observed in the plots presented in Figs. 4 to 6, the results provided by proposed framework agree with this expectation. This difference can be visualized in the simulation images provided in Fig. 7. Note the reduced visibility of the face below the blood cells (which is perpendicular to the light incidence direction) in a flow orientation in comparison with a random orientation. The increased visibility resulting from a flow orientation is associated to a higher sieve factor, *i.e.*, a higher probability of light traversing the sample without encountering any of the erythrocytes.

In order to extend our scope of observations, we also generated images depicting the different cell geometries taken into account in our *silico* experiments. As it can be observed in the images presented in Fig. 8, volume equivalent spheres take less space than randomly oriented TUC-cells. Moreover, these images show how an increase in hematocrit affects the cell count and distribution. More specifically, the increase in hematocrit increases cell count, and reduces the visibility of the face below the blood sample.

It has been mentioned in the literature [16] that the sieve effect is independent of the sample thickness. In fact, if one replaces d by t in (2), t can be eliminated from Eqs. (4) and (6). We remark, however, that such estimations may incorporate both sieve and detour effects [15, 40]. As can be observed in the images presented in Fig. 9, the visibility of the face below the blood sample is reduced when the sample thickness is increased and the hematocrit is kept constant. These visual simulations intuitively demonstrate that the probability of light traversing the medium without encountering the erythrocytes is reduced under these conditions, *i.e.*, the sieve effect decreases as the sample thickness increases.

The images presented in Fig. 9 suggest that the estimation of sieve factor can be obtained

#123519 - $15.00 USD Received 29 Jan 2010; revised 11 Mar 2010; accepted 15 Mar 2010; published 25 Mar 2010

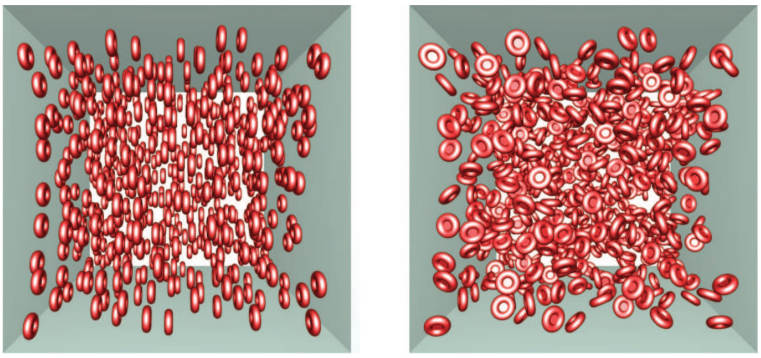

Fig. 7. Images illustrating different TUC-cell profiles as observed from viewing direction coincident with the light incidence direction. Left: flow oriented TUC-cells. Right: randomly oriented TUC-cells. These images correspond to simulations involving samples with a thickness equal to $0.1mm$ and hematocrit equal to 5%.

by computing the non-occluded area resulting from the orthographic projection of the TUC-cells. However, in order to compute this area, one would need to appropriately distribute the cells in the three-dimensional sample volume to ensure that their specific orientations and different positions (two cells cannot occupy the same space) are properly accounted for. This three-dimensional distribution may result in the overlap of the projected area of several cells. Analytical formulas to compute these areas are not straightforward since they depend on the size, shape and relative orientation of the cells, which may vary from one simulation iteration to another. Although these areas can be computed using an approximation approach (*e.g.*, by counting the number of pixels occupied by each projected area), such an approach would inherit the limitations of discrete approximations to continuous quantities. We remark that the computation of ray-cell intersections is straightforward and less prone to discretization problems, specially considering the standard primitives used in this work. Another aspect to be considered is the lack of measured data to allow a quantitative validation of different estimation approaches. Hence, the validation of a 2D area based approach should rely on direct estimations of sieve effect. As appropriately suggested by McClendon and Fukshansky (1990), direct and more accurate estimations of the sieve effect for organic tissues can be accomplished through a detailed examination of their anatomy. The proposed 3D framework was designed to contribute to this goal through the application of a first principles approach that accounts for the three-dimensional distribution of the RBCs.

4. Concluding Remarks

Theoretical and applied investigations of blood optical properties are essential for improving the reliability of techniques used in the diagnosis and treatment of several medical conditions. Nowadays, these investigations rely not only on traditional ”wet” experiments, but also on computer simulations, specially when such experiments are not feasible due to practical constraints. The efficacy of these simulations depends on the appropriate consideration of phenomena that may alter the transmission and absorption of light in blood samples. The amount of information and data describing some of these phenomena is quite scarce, however. In order to effectively contribute to the efficacy of blood optics simulations, we have specifically addressed one of these phenomena in this paper, namely the light sieve effect.

We have presented a predictive ray optics framework that can be used to quantify this effect. The proposed framework employs ray-casting techniques to compute the probability that

#123519 - $15.00 USD Received 29 Jan 2010; revised 11 Mar 2010; accepted 15 Mar 2010; published 25 Mar 2010

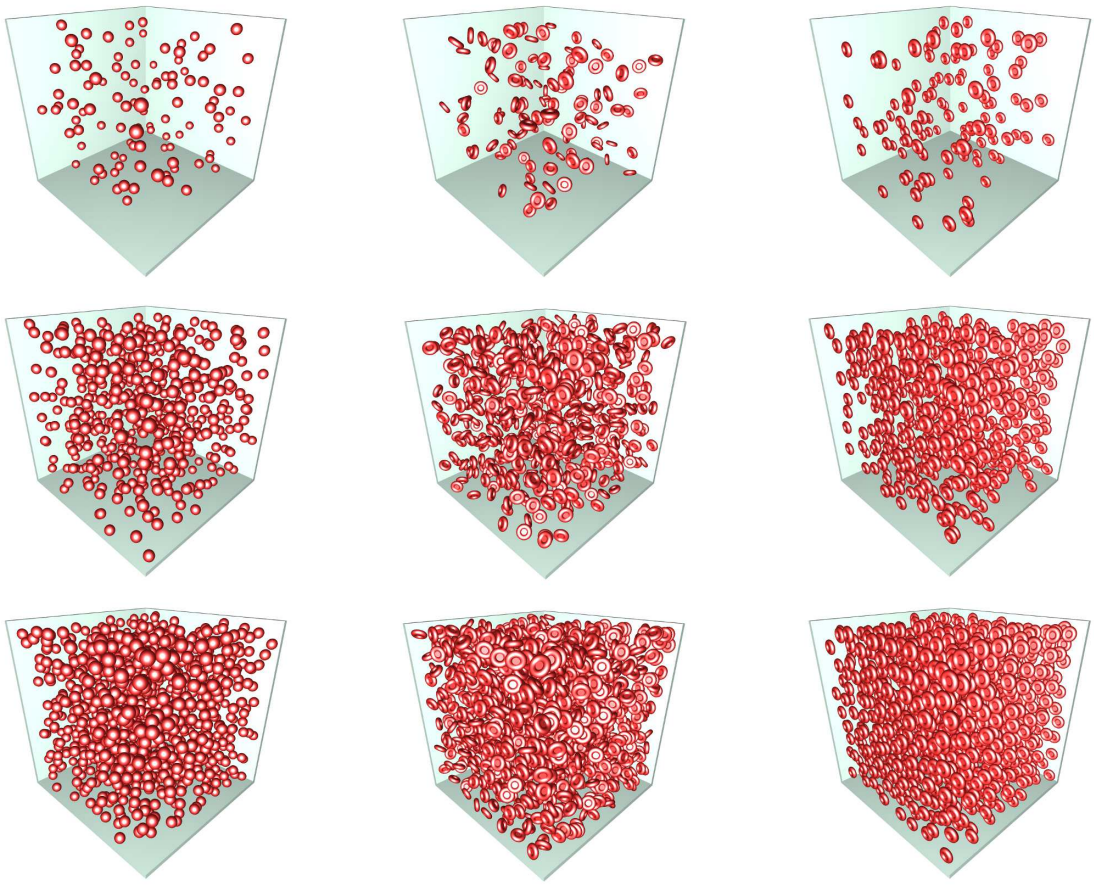

Fig. 8. Images illustrating the different cell geometries considered in the computation of the sieve effect factor. Left column: volume-equivalent spheres. Middle column: randomly-oriented TUC-cells. Right column: flow-oriented TUC-cells. Hematocrit of top row is 1%; middle row, 5%; and bottom row, 10%. These images correspond to simulations involving samples with a thickness equal to $0.1mm$ and assuming the light incidence direction to be perpendicular to the top face of the testing volume, which was removed to facilitate the visualization of the different cell geometries.

#123519 - $15.00 USD Received 29 Jan 2010; revised 11 Mar 2010; accepted 15 Mar 2010; published 25 Mar 2010

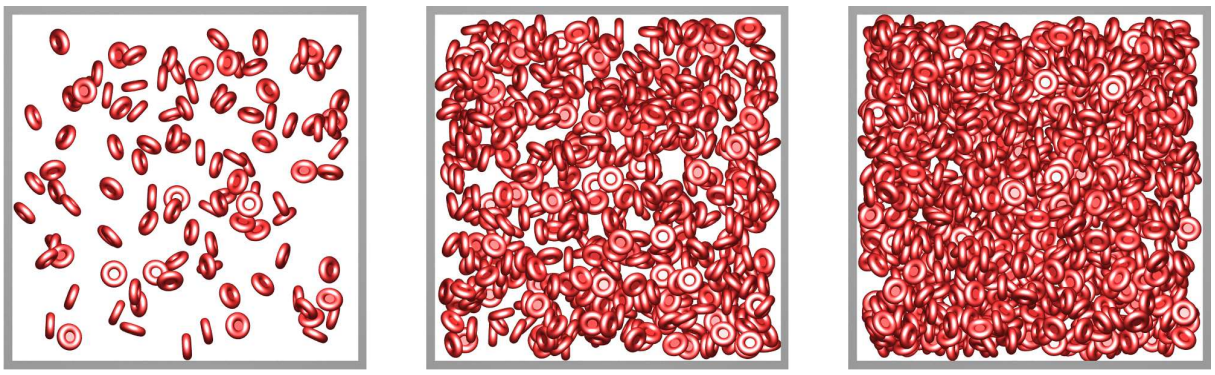

Fig. 9. Ortographic projections (perpendicular to the light incidence direction) of three blood samples with different thicknesses and the same hematocrit (1%). Left: 0.1*mm*. Middle: 0.5*mm*. Right: 1.0*mm*.

light does not intersect any erythrocyte in a sample simulating the anatomical characteristics of blood. Its predictive capabilities were demonstrated through a series of *in silico* experiments whose results qualitatively agree with observations reported in the literature. Quantitative evaluations of our simulation results were not possible due to the lack of measured data. To the best of our knowledge, no experimental measurements involving the direct quantification of sieve effects (without implicitly including detour effects) are available in the scientific literature. In fact, this constraint was one the main motivations for using a first principles approach.

It is well established that predictive *in silico* experimental frameworks may also be used to accelerate the hypothesis generation and validation cycles of research involving the behavior of biological systems [41]. Accordingly, the results of our investigation have shown that the sieve factor is affected not only by cell shape, orientation and distribution, but also by the sample thickness. With respect to the sample thickness, it was clearly demonstrated that its increase reduces the sieve effect. Although this conclusion may seem intuitive and straightforward when one observes the visualizations provided in this paper, we remark that previous investigations provided conflicting conclusions about this process [15, 16, 21].

The proposed framework is flexible and its application can be extended to different materials. For example, the TUC-cell can be replaced by other objects in order to represent other types of pigment containing structures such as the melanosomes present in human tissues and the chloroplasts present in plant tissues. It can also be extended to allow the simulation of other optical phenomena such as detour effects associated with the scattering of light by pigment containing structures. As future work, we intend to explore these research avenues and integrate the outcomes of this investigation into comprehensive models of light interaction with organic materials.

Acknowledgements

We would like to thank the anonymous reviewers for their helpful comments. The work presented in this paper was supported in part by the Natural Sciences and Engineering Research Council of Canada under grant NSERC Grant 238337.

#123519 - $15.00 USD Received 29 Jan 2010; revised 11 Mar 2010; accepted 15 Mar 2010; published 25 Mar 2010